Digital Smoothing of the Langmuir Probe I-V Characteristic

by

F. Magnus and J. T. Gudmundsson

RH-20-2002

Science Institute
University of Iceland

Digital Smoothing of the Langmuir Probe I-V Characteristic

F. Magnus and J. T. Gudmundsson,
Science Institute
University of Iceland
Dunhagi 3, IS-107 Reykjavik

September 19, 2002

Abstract

Electrostatic probes or Langmuir probes are the main diagnostic tools in plasma. From a simple Langmuir probe I-V measurement it is possible to obtain various plasma parameters and the electron energy distribution function (EEDF). To find the EEDF it is important to determine the second derivative of the I-V characteristic accurately. Any noise present in the measurement is greatly amplified by the differentiation rendering the second derivative useless unless some method of noise suppression is applied. We compare several different methods which are commonly used to smooth the I-V characteristic; a Savitzky-Golay filter, a Blackman window, a Gaussian function filter and polynomial fitting.

1 Introduction

Electrostatic probes are among the most important diagnostic devices in plasma, providing an experimentally simple method for measuring various plasma parameters. A Langmuir probe in its most basic form is simply a thin wire which is inserted into a plasma. The probe is biased at a variable voltage, positive and negative to the plasma and the current collected provides information on various plasma properties. The measured current as a function of the applied voltage is known as the probe I-V characteristic. The use of a Langmuir probe relies on efficient analysis of this I-V characteristic. From the characteristic one can determine the electron density, the electron temperature, the plasma potential and the electron energy distribution function (EEDF).

In a low pressure, weakly ionised plasma, the plasma density is only a small fraction of the neutral gas density. The applied power heats the electrons to a much greater extent than the more massive ions. Therefore the electrons have a considerably higher velocity. In low pressure, weakly ionised discharges the EEDF is generally non-Maxwellian and the electron temperature is thought of as an effective electron temperature, T_{eff}, representing the mean electron energy determined from the EEDF [1]. The insertion of a probe causes a disturbance in the plasma as electrons and ions bombard the surface and a negative charge quickly builds up on the probe. This produces a positively charged sheath and thus an electric field directed toward the probe. When the probe draws equal ion and electron currents (no net current) it is said to be at floating potential, V_{fl}. This is the potential at which any object inserted into the plasma will sit if it is floating (i.e. electrically insulated from the environment). The plasma potential, V_{pl}, is the potential at which the plasma and probe potentials are equal. From the above it is clear that the floating potential is lower than the plasma potential. These two potentials divide the I-V characteristic measured by a Langmuir probe into three regions. For a highly negative applied probe voltage, all electrons are repelled and only positive ions are attracted and collected by the probe. This is called the ion-saturation region. In the region roughly between the plasma and floating potentials the most energetic electrons reach the probe but lower-energy electrons are still repelled. This region is known as the electron-retardation region. In the electron saturation region, the probe is positive with respect to the plasma potential; the ions are fully repelled and only electrons are collected. Figure 1 shows a sample characteristic.

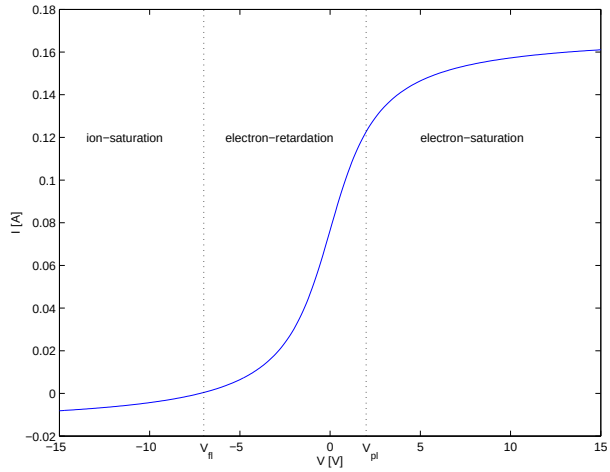

Figure 1: A typical Langmuir probe I-V characteristic. The floating potential and plasma potential divide the curve into three regions.

Determining the electron energy distribution function accurately through

experiment is very important, especially in complicated chemically reactive plasma where it is difficult to calculate the EEDF directly [2]. It has been shown that the second derivative of the I-V characteristic is proportional to the electron energy distribution function of a plasma [3]. The main challenge in the measurement of the EEDF is that the second derivative has to be accurately determined. Common methods include the use of differentiating circuits [4], ac measurements [5] and numerical differentiation [6, 7, 8, 9, 10, 11]. A plasma is a significant source of noise and in RF plasma there is additional noise due to RF interference with the probe sheath [2]. Even small errors can result in huge distortion of the EEDF as a result of the noise-amplification effect of the differentiation process. Godyak [12] points out that a dynamic range of 60 dB or more is required to analyse high energy electrons involved in ionisation and that this dynamic range can only be achieved by special filtering and averaging techniques. In other words, it is very important to develop methods to smooth the characteristic without causing further distortion before the derivative can be found. The Savitzky-Golay filter is commonly used [6, 7, 8]. Kimura et al. [9] use a finite impulse response filter that gives the second derivative via convolution. Fernández Palop et al. [10] propose the use of a Gaussian function as a filter. In an earlier work [11] we proposed the use of a Blackman window to smooth the data. In a recent study Chi et al. [4] compare direct measurement of the second derivative with applying a Gaussian filter and numerical differentiation to the I-V characteristic. They find the two methods in agreement. Here we analyse various smoothing methods and apply them to I-V probe characteristics measured in a planar inductive oxygen discharge [13] and in a high power, pulsed magnetron discharge [14]. These two systems give I-V characteristics of different lengths and noise levels. We compare the Savitzky-Golay (also known as least squares smoothing filters) and Gaussian function filters with a Blackman window smoothing filter as well as traditional polynomial fitting techniques.

2 Experimental Apparatus

The Langmuir probe measurements were carried out for two different experimental configurations at different locations. The first measurement was made at the University of California at Berkeley [13]. The setup includes a planar inductively coupled plasma source and a Langmuir probe measurement system. The plasma chamber consists of an anodised aluminium cylinder with inner diameter 30.48 cm and length 1 m. Movable aluminium pistons are at both ends. An aluminium electrode, 27 cm in diameter, is mounted on one of these pistons. The electrode serves as a wafer holder and can be water cooled. A 2.5 cm thick by 25 cm diameter quartz plate mounted on the other piston separates the planar spiral induction coil from the plasma. The

plasma is created inside a cylindrical vacuum chamber of radius $R = 15.24$ cm and length $L = 7.62$ cm and the diagnostic ports are in the mid-plane of the chamber. The source is powered at 13.56 MHz using a 1 kW Henry 1000D radio frequency power generator connected to an L-type capacitive matching network. The power supply operates in the range 0 – 1000 W. The power absorbed by the plasma was determined by first measuring the transmitted power without plasma and then subtracting that power from the power transmitted with plasma present at the same current. For all measurements the aluminium plasma chamber, electrodes and pistons are grounded.

A cylindrical Langmuir probe with a separate reference electrode is used in the experiment [2]. The measurement probe is a cylindrical tungsten rod and the probe tip length 4 mm and its radius 63.5 μm. The probe holder is an alumina tube, 0.5 mm in outer radius. The reference probe is a wire loop, 2 cm in radius made of 0.5 mm diameter tungsten wire. The reference loop is not closed and its structure is kept by an insulating holder. A sawtooth voltage with sweeping time 5 ms is applied over a 50 V range to measure the probe characteristic. The probe current $I_{\rm pr}$ is measured by sensing the voltage drop across a resistance $R_{\rm s}$. The data collected is a 1032×2 matrix containing the voltage at the circuit end of the sensor resistance, $V_{\rm c}$, and the probe current $I_{\rm pr}$.

The second measurement was made at Linköping Tekniska Högskolan, Sweden (LITH) [15]. The setup consists of a high power pulsed magnetron discharge. The standard balanced planar magnetron source is operated with a tantalum target of diameter 150 mm. The cathode is located inside a stainless steel sputtering chamber of radius $R = 60$ cm and height $L = 75$ cm. Argon of purity 99.9997 % is used as discharge gas. The argon pressure was varied from 0.5 – 20 mTorr. The magnetron cathode was driven by a pulsed power supply that can deliver peak power pulses of up to 2.4 MW (2000 V and 1200 A) at repetition frequency of 50 Hz and pulse width in the range of 50 – 100 μs. For the measurements presented here the average power was 300 W (pulse energy 6 J), pulse width 100 μs, and repetition frequency 50 Hz. The target current, target voltage and the Langmuir probe current and voltage were monitored by a Tektronix TDS 520 C (500 Mhz, 1 GS/s) oscilloscope.

The Langmuir probe used in these measurements is a cylindrical tungsten rod of length $l_{\rm pr} = (5.0 \pm 0.5)$ mm and radius $r_{\rm pr} = (50 \pm 1)$ μm. The probe holder is a 1.9 cm long alumina tube with outer radius $r_{\rm prh} = 0.5$ mm. The probe is designed to fulfil the basic requirements for Langmuir probe diagnostics as discussed by Godyak [12], $r_{\rm prh} \ll l_{\rm pr}$ and $r_{\rm pr}, r_{\rm prh}, \lambda_{\rm De} \ll \lambda_{\rm e} \sim 1$ cm. Here $\lambda_{\rm De} \sim 4-40$ μm is the Debye length and $\lambda_{\rm e} \sim 1$ cm is the electron mean free path. The probe is positioned perpendicular to the discharge axis, and thus to the electric and magnetic field lines. Close to the cathode target the electrons are strongly magnetised. The measured magnetic field 1.5 cm

below the target is 48 mT. In the substrate vicinity, 7 cm below the target the magnetic field is 0.56 mT and 20 cm below the target it has fallen to 0.13 mT. This magnetic field leads to a mean gyro radius of $a_{\rm g} = (\pi m_{\rm e} k T_{\rm e}/2)^{1/2}/eB$ and $\beta = r_{\rm pr}/a_{\rm g} \approx 0.6$ at 1.5 cm below the target, about 0.007 at 7 cm and 0.002 at 20 cm below the target. We choose the probe position so the error in the measured electron density caused by the magnetic field can be neglected [16, 17]. The probe was positioned 9 cm from the target along the centre line and positioned perpendicular to the magnetic field. The probe current was measured by finding the voltage drop across a resistance $R_{\rm s} = 10\ \Omega$. The time resolved probe current was recorded for 500 μs or 1000 μs after initiating the pulse at 1 μs or 2 μs intervals for a fixed voltage. This was repeated in the voltage range -10 V to 15 V. For each time value the I-V curve was reconstructed. Thus, each data set (for each time value) is a 126×2 matrix containing the voltage at the probe end of the sensor resistance and the probe current.

3 Langmuir Probe Diagnostics

The second derivative of the I-V probe characteristic is calculated and the electron energy distribution function $g_{\rm e}(\mathcal{E})$ is found. The electron energy distribution function (EEDF) is given by the Druyvesteyn formula as [3, 18]

$$g_{\rm e}(V) = \frac{2m}{e^2 A_{pr}} \left(\frac{2eV}{m}\right)^{1/2} \frac{d^2 I_{\rm e}}{dV^2} \tag{1}$$

and the electron energy probability function (EEPF) is

$$g_p(\mathcal{E}) = \mathcal{E}^{-1/2} g_{\rm e}(\mathcal{E}) \tag{2}$$

where $\mathcal{E}$ is the electron energy in equivalent voltage units. The plasma potential $V_{\rm pl}$ is the voltage where the second derivative of the electron current $I_{\rm e}$ is zero or the voltage at the first derivative maximum. The electron density $n_{\rm e}$ is determined as

$$n_{\rm e} = \int_0^\infty g_{\rm e}(\mathcal{E}) d\mathcal{E} \tag{3}$$

and the effective electron temperature $T_{\rm eff}$ is determined by

$$T_{\rm eff} = \frac{1}{n_{\rm e}} \frac{2}{3} \int_0^\infty \mathcal{E} g_{\rm e}(\mathcal{E}) d\mathcal{E} \tag{4}$$

We will find that the smoothing methods introduce distortion to the electron energy distribution function. To minimise the effect of this distortion on the electron density and effective electron temperature, the measured electron energy distribution functions are fitted to the function $g_R(\mathcal{E}) = a\sqrt{\mathcal{E}} \exp(-b\mathcal{E}^x)$ where a, b and x are constants. The Maxwellian electron energy distribution

is a special case with $x = 1$ and the Druyvesteyn distribution is a special case with $x = 2$. The value of x was determined by performing a least-squares analysis of $\ln(g_R(\mathcal{E})/\sqrt{\mathcal{E}})$ versus $\mathcal{E}^x$ for various x to find the best fit. The maximum of the electron energy distribution function is found and the corresponding electron energy. The equation is fitted to the measured electron energy distribution function from the electron energy where the electron energy distribution function has maximum value until it has fallen two orders of magnitude. The best fit to the equation is then interpolated to zero electron energy, and the electron density and effective electron temperature are calculated.

4 Smoothing Methods

It is our aim to calculate the EEDF from the second derivative of the smoothed I-V characteristic. In this section we will compare three different filtering methods; a Gaussian function filter, a Blackman window and a Savitzky-Golay filter. Furthermore, we compare filtering to fitting methods.

In order to compare the methods we construct the following test function:

$$f(x) = \frac{\arctan(\frac{1}{2}x) + 1.3}{17} \tag{5}$$

This function closely resembles an actual measured I-V characteristic where the values 1.3 and 17 are chosen to give the correct positioning and scale. Figure 1 shows the test function. It might be equally effective to use a combination of tanh and arctan in order to attain a flat negative region and an increasing positive region but for simplicity we choose equation (5). We will perform the filtering on two lengths of the test function; 1032 points and 126 points uniformly distributed on the interval $[-10, 15]$ in order to simulate the Berkeley data and the LITH data respectively. Next we add random Gaussian noise to the test function using the Matlab function `randn`. The noise level is determined by fitting a polynomial separately to the electron- and ion-saturation regions of a measured characteristic. The difference between the fitted polynomial and the measured function gives a rough estimate of the noise. Testing shows that the Berkeley data has noise with a standard deviation of less than 1×10^{-4} and the LITH data approximately 1×10^{-3}. We will test the filters for both sizes and noise levels and give the function $f(x)$ the subscripts 'L' and 'S' to denote large and small. The filtered data will be denoted by y and the same subscripts.

There are various ways to compare the methods. One possibility is simply to find the smallest mean-square difference between the filtered and original functions or their derivatives. However, we are primarily interested in the region where the probe potential, V_p, is below the plasma potential and in accurately deriving the second derivative maximum. The mean-square

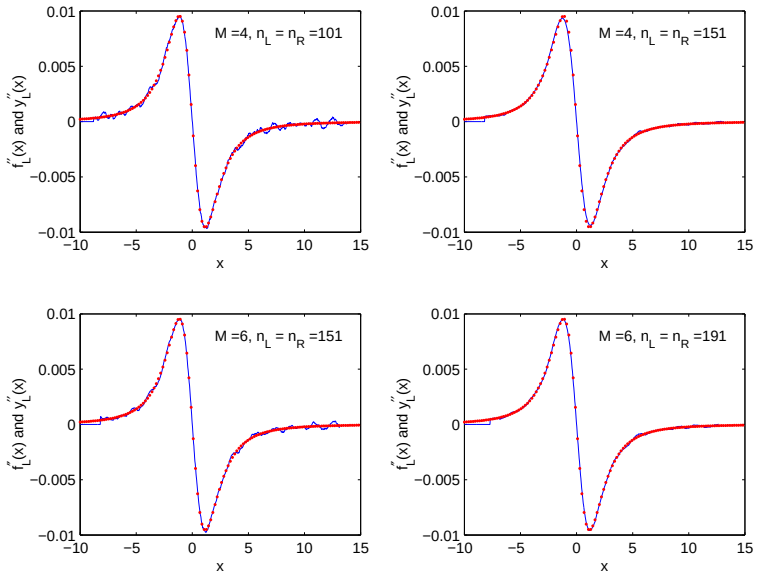

Figure 2: Second derivatives of the Savitzky-Golay filtered function and $f_{\mathrm{L}}(x)$ for various values of M and $n_{\mathrm{L}} = n_{\mathrm{R}}$. The dotted curve is the noise-less derivative. Data vector length: 1032

difference over the whole range of V_{p} may therefore not be the most important factor. It is therefore useful to plot the error as a function of voltage. This gives a clear picture of the distribution of error. Another possibility is to find the correlation coefficient of the second derivative of the filtered and original signals. If the signals are identical (i.e. the filter has completely removed the noise) the correlation coefficient is equal to one. The highest correlation coefficient might therefore give the optimum filter. The final method is to compare the curves visually. This has the advantage that it is possible to pick the smoothing method which gives the closest fit in the areas which we deem most important. However, in some cases it may be difficult to choose between two images which are similar without any quantitative results. In most cases we will use a combination of the methods above.

For all filters we will vary the filter parameters to determine the optimum configuration. Only a few values will be shown. These are determined by finding the minimum mean-square value and maximum correlation coefficient and looking at an interval approximately centred at these values.

4.1 Savitzky-Golay Filter

This smoothing technique was introduced by A. Savitzky and M. J. E. Golay in 1964 [19]. The idea is to approximate the underlying function within a moving window with a polynomial of degree two or higher. For each point x_i

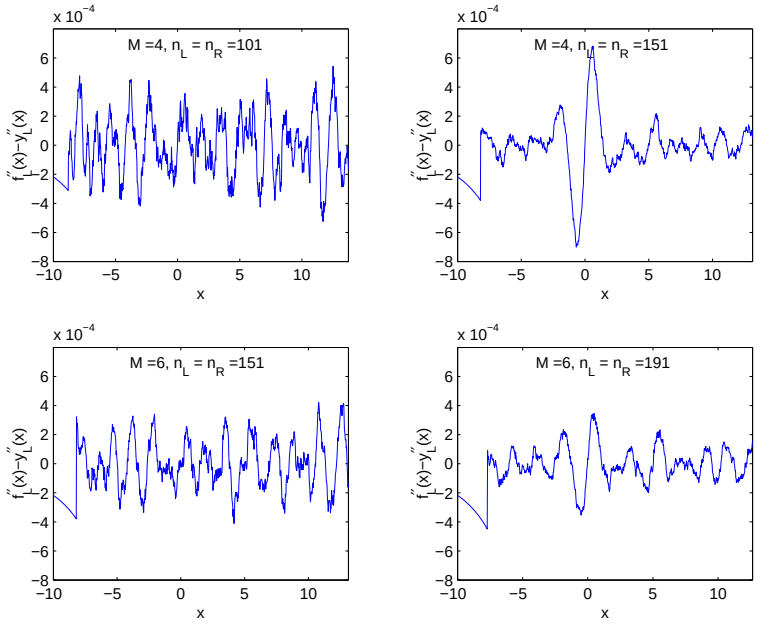

Figure 3: Difference between the second derivatives of the Savitzky-Golay filtered function and $f_{\mathrm{L}}(x)$. Data vector length: 1032

of the function to be smoothed we fit a polynomial through $n_{\mathrm{L}}+n_{\mathrm{R}}+1$ points centred at x_i where n_{L} and n_{R} denote the number of points to the left and right of x_i respectively. In what follows we will assume $n_{\mathrm{L}} = n_{\mathrm{R}}$. The value of the polynomial at x_i gives the smoothed value g_i at that point and the other values of the polynomial are discarded. Therefore, the Savitzky-Golay filter has three parameters: n_{L}, n_{R} and the degree of the polynomial, M. It is not obvious how to choose these parameters and in many cases some visual optimisation is required in order to obtain the best results. This is one of the disadvantages of the method [20]. A wide window (n_{L} and n_{R} large) will result in more smoothing but at the cost of more distortion of higher frequency content. In contrast, higher-order filters can track narrower features but with loss of smoothing of low frequency content [21]. More guidelines for the choice of parameters are given by Press and Teukolsky [21].

Savitzky-Golay filters are typically used for smoothing of signals whose frequency span is large. In general, they are not as effective at rejecting noise as standard averaging filters. However, the Savitzky-Golay filtering method has the advantage that it is easy to determine the second derivative directly. One need only find the derivative of each polynomial at the centre point. This approach will be adopted here. The filtering introduces distortion at the edges so we set the first and last $(n_{\mathrm{L}}+1)/2$ points to zero. It should be noted that the Savitzky-Golay method strictly only applies to data points

M	$n_{\mathrm{L}} = 81$	$n_{\mathrm{L}} = 101$	$n_{\mathrm{L}} = 151$	$n_{\mathrm{L}} = 191$	$n_{\mathrm{L}} = 251$
2	9.2×10^{-8}	1.9×10^{-7}	7.0×10^{-7}	1.4×10^{-6}	2.9×10^{-6}
4	1.2×10^{-7}	4.3×10^{-8}	3.7×10^{-8}	1.2×10^{-7}	4.3×10^{-7}
6	5.2×10^{-7}	2.1×10^{-7}	3.2×10^{-8}	2.3×10^{-8}	7.4×10^{-8}

Table 1: Mean-square error for the large data set $f_{\mathrm{L}}(x)$ using the Savitzky-Golay filter. Data vector length: 1032

M	$n_{\mathrm{L}} = 81$	$n_{\mathrm{L}} = 101$	$n_{\mathrm{L}} = 151$	$n_{\mathrm{L}} = 191$	$n_{\mathrm{L}} = 251$
2	0.9978	0.9957	0.9837	0.9662	0.9277
4	0.9958	0.9985	0.9988	0.9966	0.9877
6	0.9823	0.9929	0.9989	0.9993	0.9978

Table 2: Correlation coefficient for $f_{\mathrm{L}}(x)$ using the Savitzky-Golay filter. Data vector length: 1032

which are equally spaced in the independent variable. However, assuming that the data points *are* equally spaced simply amounts to shifting of each point to equally spaced positions. This is equivalent to adding noise to the function which may be acceptable if it is much smaller than the noise already present [21].

Table 1 shows the mean-square difference between the second derivatives of the filtered function and $f_{\mathrm{L}}(x)$ for different values of $n_{\mathrm{L}} = n_{\mathrm{R}}$ and M. Table 2 shows the correlation coefficient of the derivatives of the filtered function and $f_{\mathrm{L}}(x)$. Figure 2 shows the second derivatives for the best filter parameters and figure 3 shows the difference of the two. The figures are consistent with the mean-square and correlation coefficient values. All configurations give good results and we can see that the error is evenly distributed for all except $M = 4$, $n_{\mathrm{L}} = 151$ where the maximum and minimum have been flattened slightly. The lowest error is for $M = 6$, $n_{\mathrm{L}} = 191$ but this large window also produces a large distortion band at the edge.

Tables 3 and 4 show the second derivative mean-square error and correlation coefficient for the small data set, $f_{\mathrm{S}}(x)$. As expected these values are not as good as the ones obtained from the large data set as the level of noise is also higher. The best results are for $M = 8$ and $n_{\mathrm{L}} = 45$. Figure 4 shows the results for the best filter parameters and figure 5 shows the error. As expected, the choice of the parameters n_{L}, n_{R} and M, depends on the length of the data and the noise level. For $n_{\mathrm{L}} = 45$ the distortion region at the edge is quite large and might be considered unacceptable. For this reason it is not practical to use larger windows.

M	$n_\mathrm{L} = 25$	$n_\mathrm{L} = 29$	$n_\mathrm{L} = 33$	$n_\mathrm{L} = 37$	$n_\mathrm{L} = 45$
4	8.6×10^{-7}	7.3×10^{-7}	8.1×10^{-7}	1.0×10^{-6}	1.9×10^{-6}
6	2.8×10^{-6}	1.4×10^{-6}	9.6×10^{-7}	8.3×10^{-7}	8.0×10^{-7}
8	1.0×10^{-5}	3.7×10^{-6}	1.6×10^{-6}	9.4×10^{-7}	5.6×10^{-7}

Table 3: Mean-square error for the small data set $f_\mathrm{S}(x)$ using the Savitzky-Golay filter. Data vector length: 126

M	$n_\mathrm{L} = 25$	$n_\mathrm{L} = 29$	$n_\mathrm{L} = 33$	$n_\mathrm{L} = 37$	$n_\mathrm{L} = 45$
4	0.9789	0.9804	0.9763	0.9690	0.9473
6	0.9377	0.9700	0.9796	0.9818	0.9763
8	0.7738	0.8978	0.9531	0.9715	0.9835

Table 4: Correlation coefficient for $f_\mathrm{S}(x)$ using the Savitzky-Golay filter. Data vector length: 126

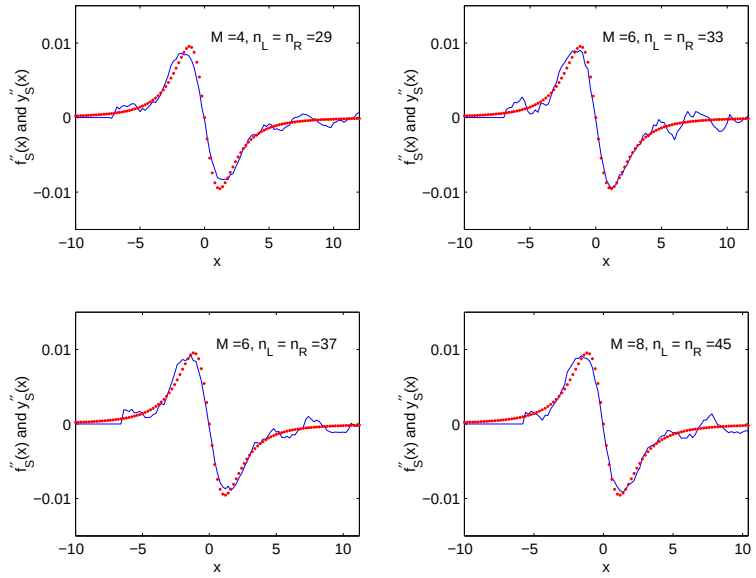

Figure 4: Second derivatives of the Savitzky-Golay filtered function and $f_\mathrm{S}(x)$ for various values of M and $n_\mathrm{L} = n_\mathrm{R}$. Data vector length: 126

4.2 Gaussian Filter

Hayden [22] introduced a simple data-smoothing algorithm that utilises a Gaussian distribution function as a filter. Fernández Palop et al. [10] apply this filter to smooth the Langmuir probe I-V characteristic and compare it to the Savitzky-Golay filter and B-spline approximation. They conclude that the Hayden method has considerable advantages over the other two. The

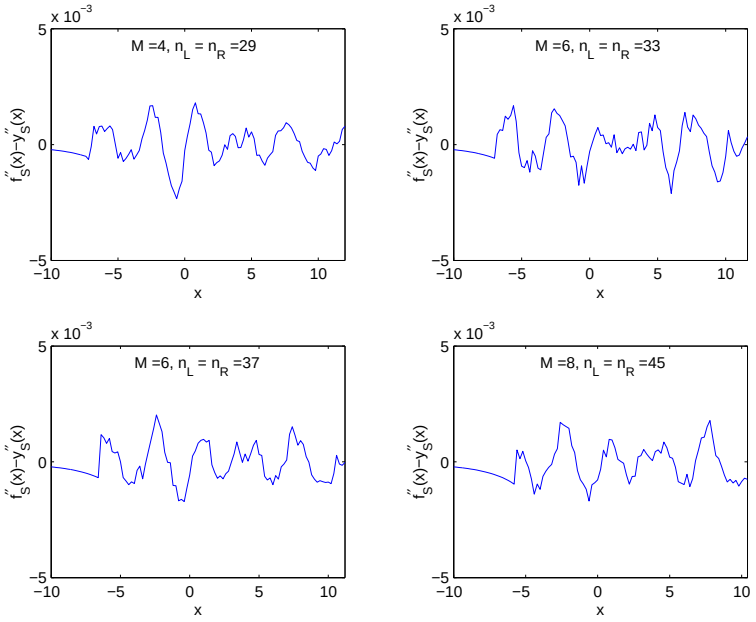

Figure 5: Difference between the second derivatives of the Savitzky-Golay filtered function and $f_{\mathrm{S}}(x)$. Data vector length: 126

n-th approximation to the original function can be found from the convolution of the measured data and the instrument function, g_n, which is usually known as the filter function. In most cases the instrument function can be approximated by a Gaussian function. The Gaussian filter function is given by

$$g_n(x) = \sum_{k=1}^{n} \binom{n}{k} (-1)^{k+1} \frac{1}{\sigma\sqrt{2\pi k}} e^{\frac{-x^2}{2\sigma^2 k^2}} \tag{6}$$

where n is the number of iterations and σ is the standard deviation. This is not the standard Gaussian window because the width of g_n is fixed and is the same as the length of the data. The number of iterations is chosen to be equal to one and the standard deviation is varied to determine the degree of smoothing. The second derivative is calculated from the filtered data using the central difference approximation.

Table 5 shows the mean-square error in the second derivative and the correlation coefficient after applying the Gaussian filter to $f_{\mathrm{L}}(x)$. The best results are obtained for $\sigma = 0.3$ which gives the lowest mean-square error and highest correlation coefficient. Figure 6 shows the second derivatives of the filtered and original functions and Figure 7 shows the difference of the second derivatives. From the figures it is apparent that for $\sigma = 0.3$ there is slight distortion of the maximum and minimum whereas $\sigma = 0.25$ produces evenly distributed low error.

Table 6 shows the mean-square error and correlation coefficient for $f_{\mathrm{S}}(x)$.

σ	Mean-square error.	Correlation coefficient
0.2	2.1×10^{-7}	0.9943
0.25	9.6×10^{-8}	0.9976
0.3	8.0×10^{-8}	0.9983
0.4	1.5×10^{-7}	0.9975

Table 5: Mean-square error and correlation coefficient for $f_{\mathrm{L}}(x)$ using the Gaussian filter. Data vector length: 1032

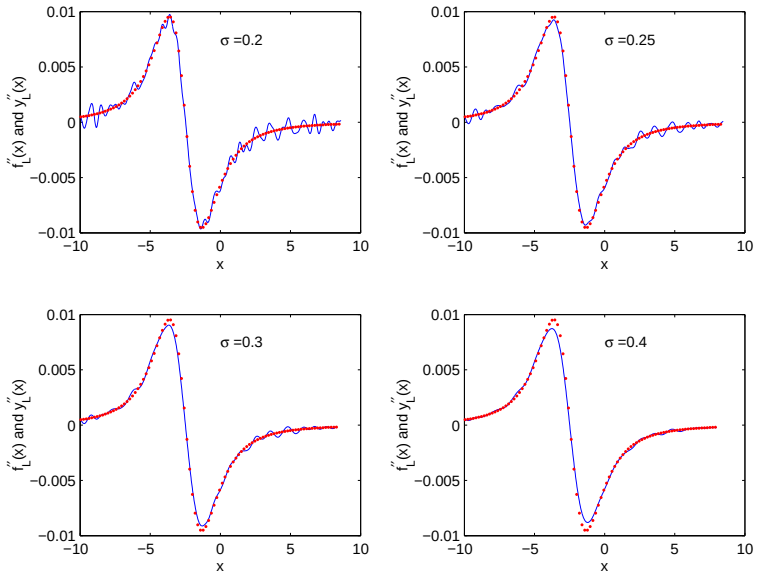

Figure 6: Second derivatives of the Gaussian filtered function and $f_{\mathrm{L}}(x)$. Data vector length: 1032

The best results are for $\sigma = 0.6$ although not nearly as good as before. Figures 8 and 9 show that there is still a considerable amount of noise in the data. In order to obtain a reasonable degree of smoothing one must settle for considerable distortion of the maximum and minimum. This is apparent from figure 9.

4.3 Blackman Window

The Blackman window is given by [23]

$$w_B(n) = 0.42 - 0.5\cos\frac{2\pi n}{M} + 0.08\cos\frac{4\pi n}{M}, \qquad n = 0, 1, 2, \ldots, M \tag{7}$$

where M is the size of the window and controls the degree of smoothing. The Blackman window minimises the side-lobe level while having a steep

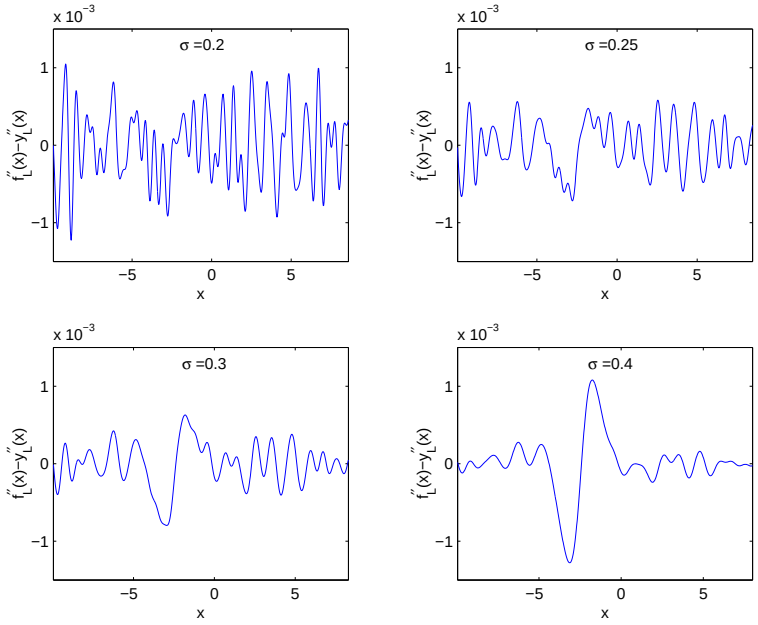

Figure 7: Difference between the second derivatives of the Gaussian filtered function and $f_{\mathrm{L}}(x)$. Data vector length: 1032

σ	Mean-square error.	Correlation coefficient
0.5	1.2×10^{-6}	0.9616
0.6	9.2×10^{-7}	0.9750
0.7	1.0×10^{-6}	0.9758
0.75	1.1×10^{-6}	0.9742

Table 6: Mean-square error and correlation coefficient for $f_{\mathrm{S}}(x)$ using the Gaussian filter. Data vector length: 126

roll-off on the side-lobes. This is a standard moving average window and the filtering is extremely easy to implement in Matlab. The derivative is found by applying the central difference approximation. However, it might be possible to eliminate the error introduced by numerical differentiation by differentiating equation (7) analytically and combining the filtering and differentiation in one convolution. As usual, the signal is shifted by $(M-1)/2$ samples and there are distortion bands of length $M-1$ at the beginning and end.

Table 7 shows the mean-square error and correlation coefficient of the second derivative of the smoothed numerically simulated I-V characteristic for different values of M. Figure 10 shows the curves and figure 11 the error. As we can see from Figure 10 lower values of M maintain the shape

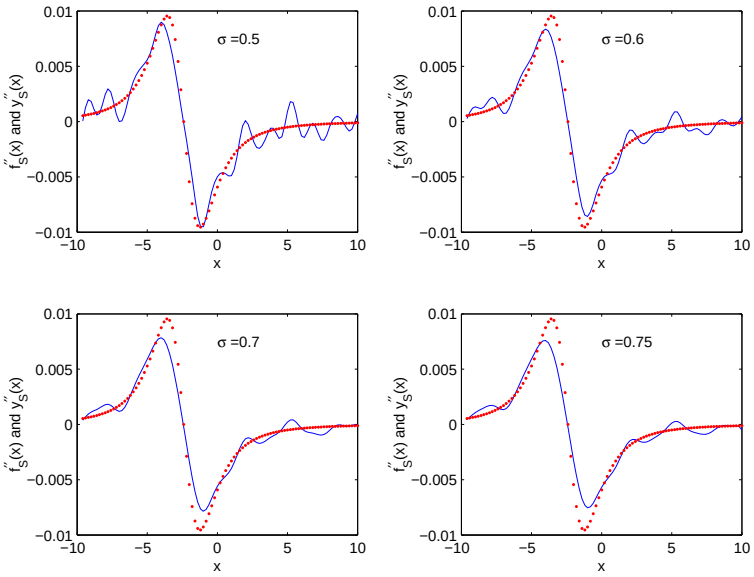

Figure 8: Second derivatives of the Gaussian filtered function and $f_{\mathrm{S}}(x)$. Data vector length: 126

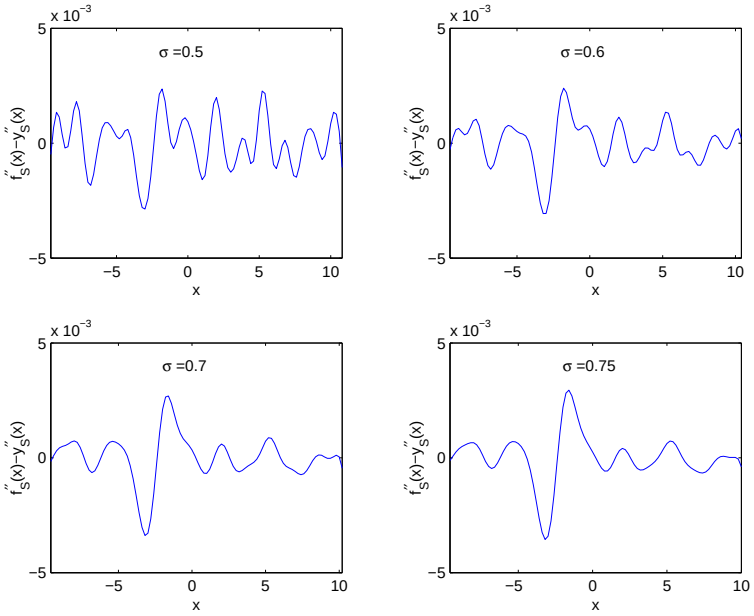

Figure 9: Difference between the second derivatives of the Gaussian filtered function and $f_{\mathrm{S}}(x)$. Data vector length: 126

of the maximum and minimum but with less smoothing. $M = 81$ gives the lowest mean-square error value and the highest correlation coefficient. On average the mean-square values are slightly higher than for the Savitzky-

Golay and Gaussian function filters. As would be expected the filter flattens the maximum and minimum slightly for all parameter values.

M	Mean-square error	Correlation coefficient
71	1.3×10^{-7}	0.9959
81	1.2×10^{-7}	0.9963
91	1.3×10^{-7}	0.9962
101	1.6×10^{-7}	0.9958

Table 7: Mean-square error and correlation coefficient using the Blackman window on $f_{\mathrm{L}}(x)$. Data vector length: 1032

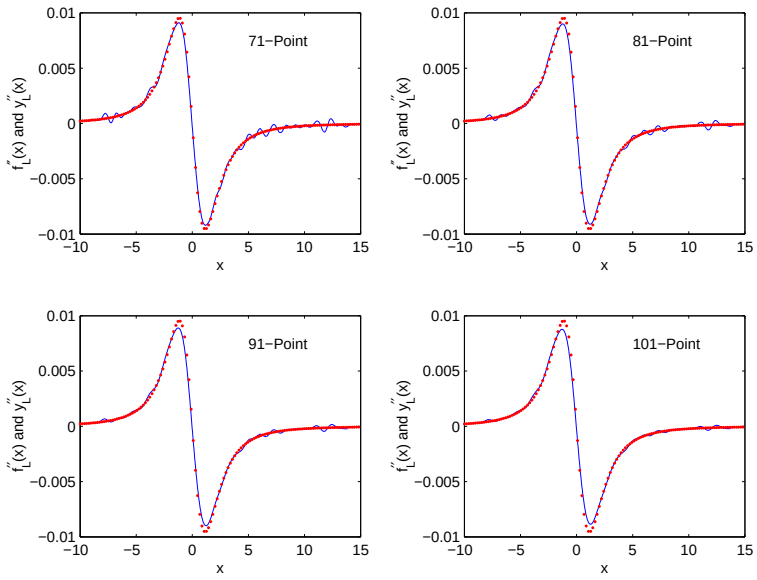

Figure 10: Second derivatives of the Blackman window filtered function and $f_{\mathrm{L}}(x)$. Data vector length: 1032

Table 8 shows the mean-square error and correlation coefficient for the small noisy data set, $f_{\mathrm{S}}(x)$, for different values of M. The mean-square values are consistently one decade higher than for the longer data and slightly higher than for the Gaussian filter. Figures 12 and 13 show the second derivatives and error. The results are very similar to those for the Gaussian filter.

4.4 Polynomial Fitting

The final method tested is to fit a polynomial of degree n to the noisy function using the method of least squares. Polynomial fits are particularly attractive

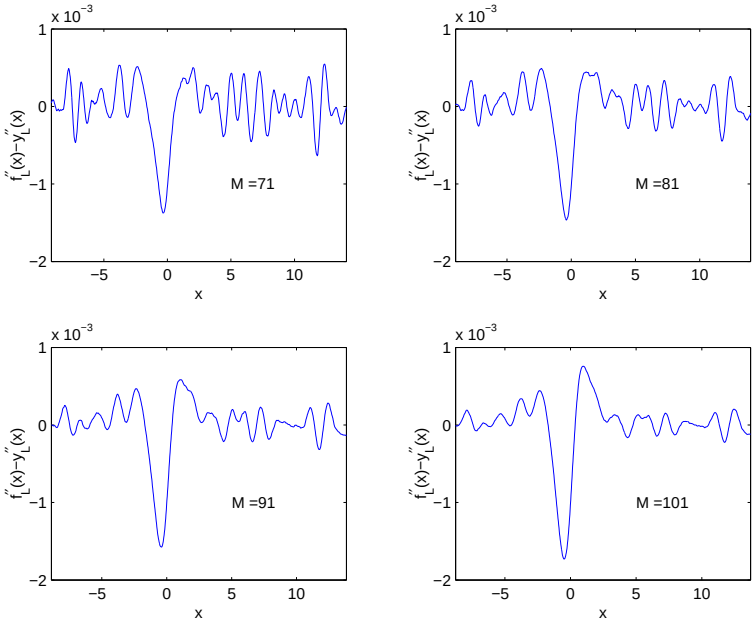

Figure 11: Difference between the second derivatives of the Blackman filtered function and $f_{\mathrm{L}}(x)$. Data vector length: 1032

M	Mean-square error	Correlation coefficient
16	3.9×10^{-6}	0.8647
19	2.6×10^{-6}	0.9082
22	3.2×10^{-6}	0.8873
28	3.4×10^{-6}	0.8877

Table 8: Mean-square error and correlation coefficient using the Blackman window on $f_{\mathrm{S}}(x)$. Data vector length: 126

because they can be differentiated (or integrated) easily. The method is also extremely easy to adapt to different lengths of data and different noise intensities.

Table 9 shows the second derivative mean-square error and correlation coefficient for different values of n for the larger data set. These results are similar to the Gaussian function results. Figures 14 and 15 show the derivatives and their difference, respectively. The fitted functions follow the maximum and minimum exceptionally well but there is significant distortion around the edges.

The second derivative mean-square error and correlation coefficient for the smaller data set, $f_{\mathrm{S}}(x)$, are shown in table 10. Figures 16 and 17 show the results of the filtering. As with the larger data set the maximum and

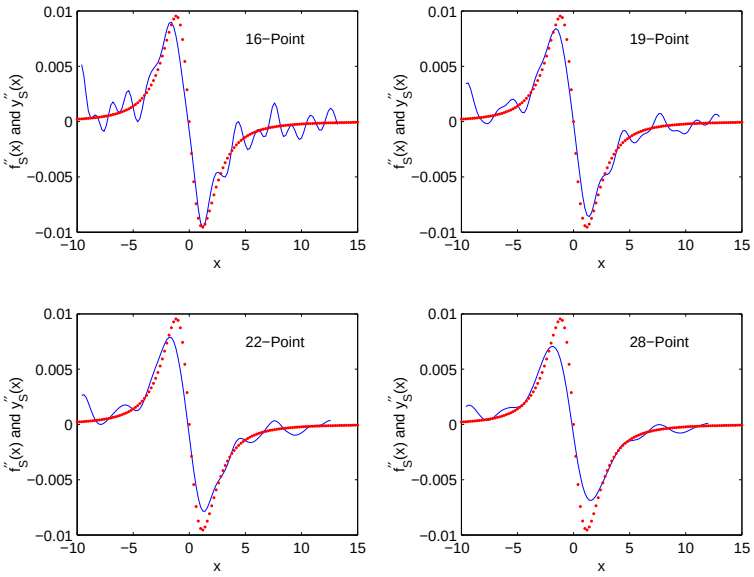

Figure 12: Second derivatives of the Blackman window filtered function and $f_{\mathrm{S}}(x)$. Data vector length: 126

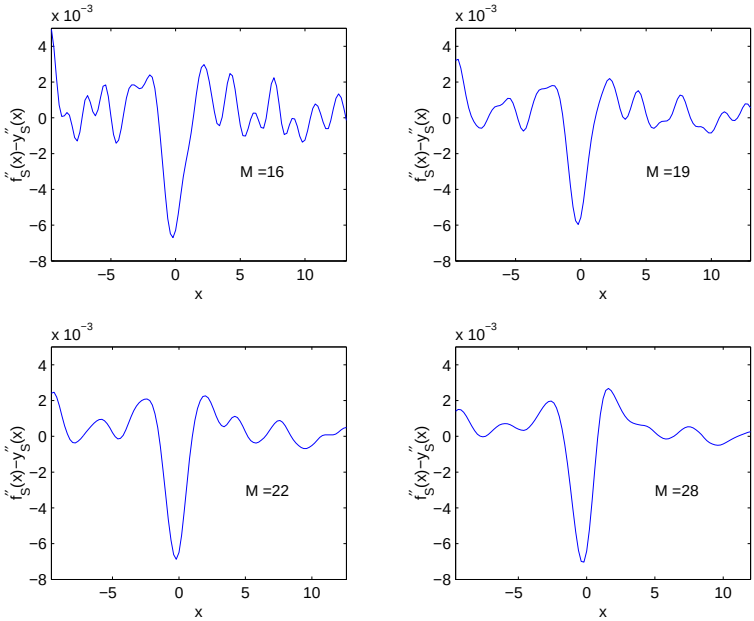

Figure 13: Difference between the second derivatives of the Blackman filtered function and $f_{\mathrm{S}}(x)$. Data vector length: 126

minimum are reproduced quite accurately whereas there is considerable distortion at the edges.

n	Mean-square of error	Correlation coefficient
29	1.3×10^{-7}	0.9953
33	8.1×10^{-8}	0.9972
36	7.7×10^{-8}	0.9974
39	4.2×10^{-7}	0.9857

Table 9: Mean-square error and correlation coefficient for $f_{\mathrm{L}}(x)$ using polynomial fitting. Data vector length: 1032

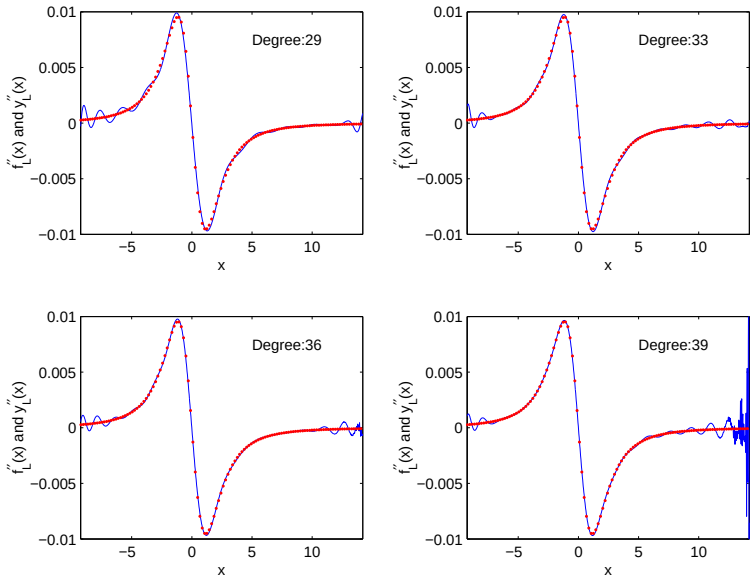

Figure 14: Second derivatives of the fitted function and $f_{\mathrm{L}}(x)$. Data vector length: 1032

4.5 Summary

All methods give good results for the larger data set. The Savitzky-Golay filter produces the best mean-square and correlation coefficient values and as can be seen from figure 2, achieves excellent smoothing without distorting the higher frequency content of the characteristic. However, the difference between the methods is small.

The results are not as good for the shorter data set. The Savitzky-Golay still has the best mean-square and correlation coefficient values but figure 4 shows that the result is far from being smooth. For higher levels of noise this method might not be practical keeping in mind that it is primarily used for noise suppression of low noise, high frequency content signals. The Gaussian filter and Blackman window produce slightly smoother curves although with more distortion. The results from polynomial fitting were not satisfactory.

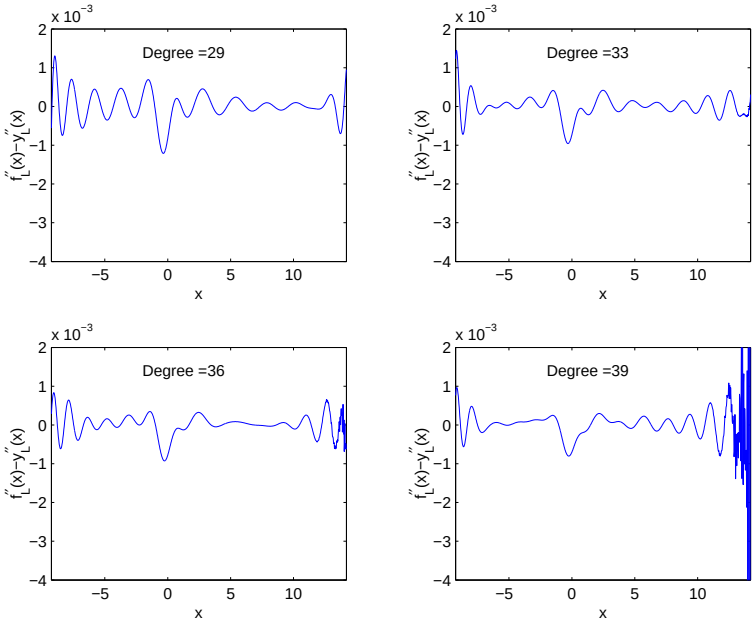

Figure 15: Difference between the second derivatives of the fitted function and $f_{\mathrm{L}}(x)$. Data vector length: 1032

n	Mean-square of error	Correlation coefficient
15	4.1×10^{-6}	0.8733
17	3.4×10^{-6}	0.8959
21	2.9×10^{-6}	0.9114
25	3.7×10^{-6}	0.8900

Table 10: Mean-square error and correlation coefficient for $f_{\mathrm{S}}(x)$ using polynomial fitting. Data vector length: 126

It should be noted that there is always a compromise between accurately producing the electron energy distribution function maximum or the high-energy electron tail. Larger windows flatten the maximum while achieving good smoothing for higher energies and small windows retain the shape of the maximum with less smoothing for higher energies. As a result it may be necessary to use a combination of filtering and fitting methods as described in section 3.

5 Experimental Results

Finally we apply the methods tested to measured data. The experimental setup is described in section 2. The filtering and calculations are implemented

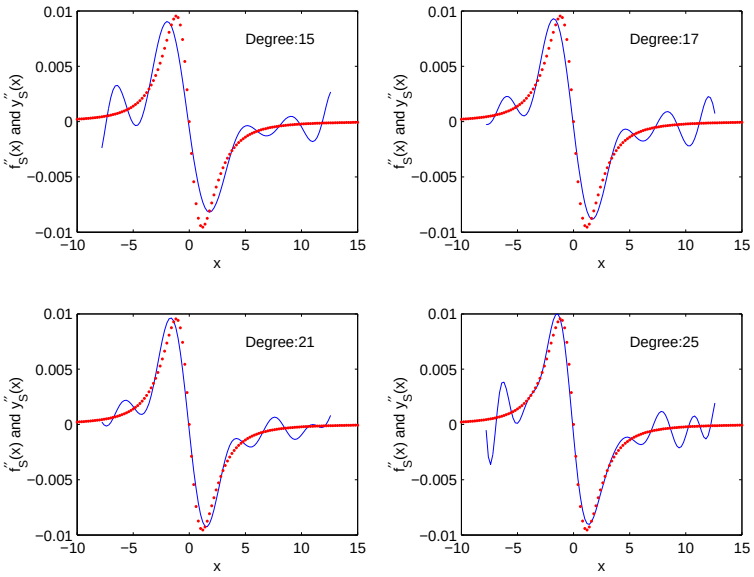

Figure 16: Second derivatives of the fitted function and $f_{\mathrm{S}}(x)$. Data vector length: 126

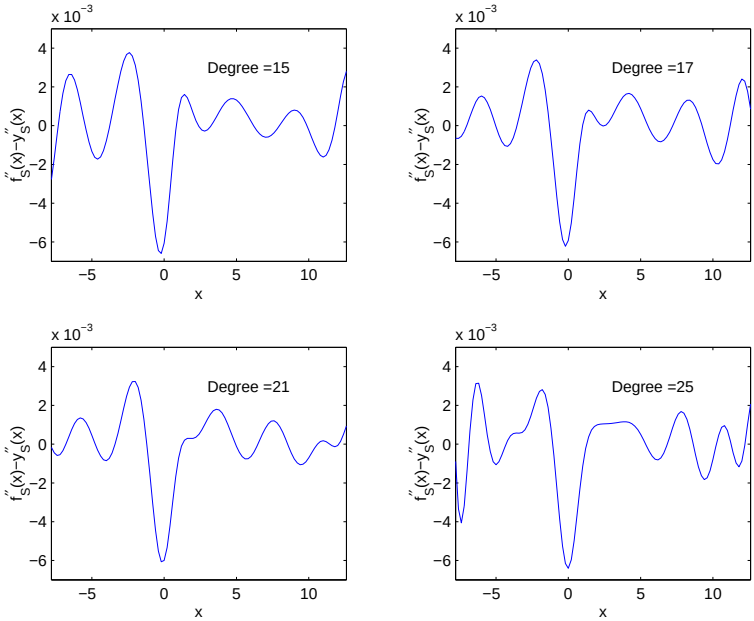

Figure 17: Difference between the second derivatives of the fitted function and $f_{\mathrm{S}}(x)$. Data vector length: 126

in a Matlab script. The script reads the data from a file, performs the filtering and finds the first and second derivatives directly in the case of the

Savitzky-Golay method or by the central difference approximation for the other methods. It then calculates the plasma parameters as discussed in section 3.

In both the experimental layouts, the probe current is found from the voltage across the resistance R_s. Let V_c and V_s be the voltages at the circuit and probe ends of R_s, respectively. In the case of the Berkeley data the voltage collected is V_c and it is therefore necessary to correct for the potential drop across the sensor resistance in order to obtain the true probe I-V characteristic. The simplest correction method is to subtract the potential drop, $I_\mathrm{pr}R_\mathrm{s}$, from V_c, thus obtaining V_p. This method is fine for the Gaussian filter, the Blackman window filter and polynomial fitting. However, the Savitzky-Golay method demands that the data points be equally spaced in the independent variable and although V_c is approximately equally spaced, V_p is not, because the Langmuir probe current is not a linear function of the bias voltage. To bypass this problem Sudit and Woods [7] propose a method for determining the first or second derivatives of the probe characteristic through the derivatives of the probe current with respect to the equally spaced voltage V_c. The first derivative is found using the equation

$$\frac{dI_p}{dV_p} = \frac{dI_p}{dV_c}\left(1 - R_c\frac{dI_p}{dV_c}\right)^{-1} \tag{8}$$

and similarly the second derivative can be found from

$$\frac{d^2I_p}{dV_p^2} = \frac{d^2I_p}{dV_c^2}\left(1 - R_c\frac{dI_p}{dV_c}\right)^{-3}. \tag{9}$$

The LITH data, on the other hand, contains the probe voltage V_p and is not equally spaced. To use the Savitzky-Golay method we must therefore first add the potential drop across R_s before filtering and finally apply equations (8) and (9) to correct for R_s. The other smoothing methods can however be applied directly to the LITH data without modifications.

Figure 18 shows the second derivative of the larger data set measured at Berkeley after being smoothed by each of the four methods. The discharge is a 43% O_2/57% Ar mixture at 7 mTorr pressure and the applied power is roughly 550 W. Figure 19 is a logarithmic plot of the electron energy probability function derived from the Druyvesteyn formula (equation (1)) and equation (2). The Savitzky-Golay, Gauss and Blackman methods produce similar results. However, the Savitzky-Golay gives the sharpest maximum which is probably more accurate but the Gauss and Blackman methods show a much sharper minimum. This is not as important, though, because the minimum is not used to calculate the EEDF and EEPF. Polynomial fitting gives a reasonable picture of the second derivative but the EEPF is unacceptable. We can see that the results are meaningless for energies above approximately 15 eV. In this region the second derivative hovers around zero. Taking the

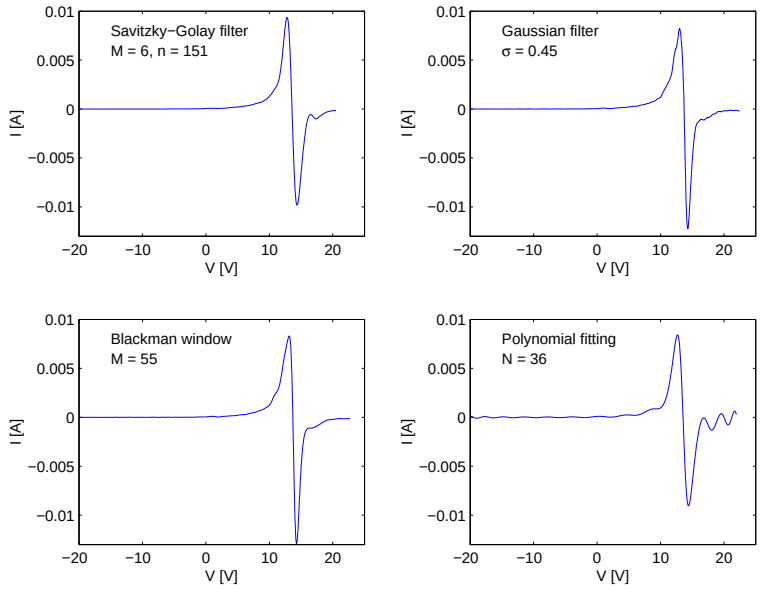

Figure 18: The second derivative of the Berkeley data set after smoothing by each of the methods.

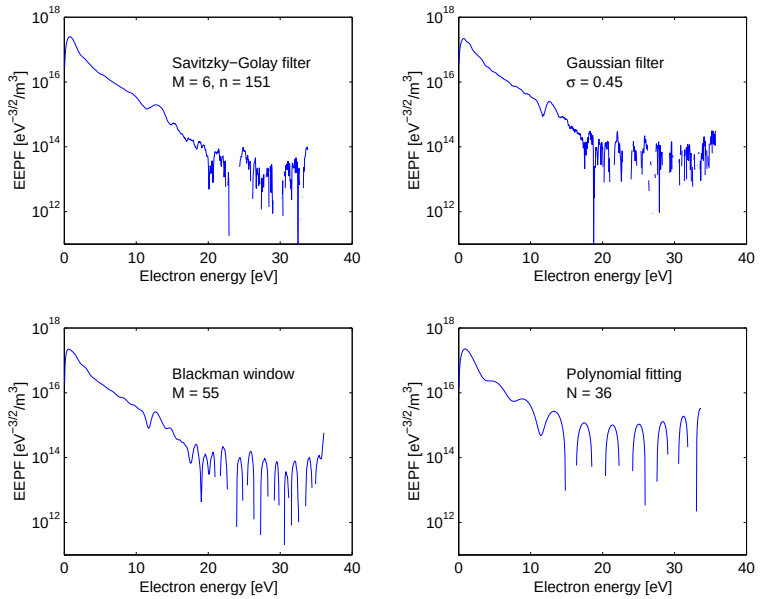

Figure 19: The electron energy probability function of the smoothed Berkeley data.

logarithm magnifies the error producing gaps in the plots where the derivative is negative. It is interesting to note that there is a bump in the EEPF around 12 eV in all the figures. The filter parameters giving optimum results

Method	T_{eff} [eV]	$T_{\text{eff}}^{\text{fit}}$ [eV]
Savitzky-Golay	3.3396	2.2246
Gaussian function	3.4573	2.2614
Blackman window	3.4756	2.2828
Polynomial fitting	3.4704	2.1507

Table 11: The effective electron temperature for the Berkeley data

differ somewhat from the ones determined in section 4. The reason might be that in reality the noise is not strictly Gaussian.

Table 11 shows the effective electron temperature calculated from the filtered data (T_{eff}) and from a fit to the electron energy distribution function interpolated down to low energy electrons ($T_{\text{eff}}^{\text{fit}}$) as described in section 3. The results are similar for all methods and $T_{\text{eff}}^{\text{fit}}$ is approximately 34 % lower than T_{eff}.

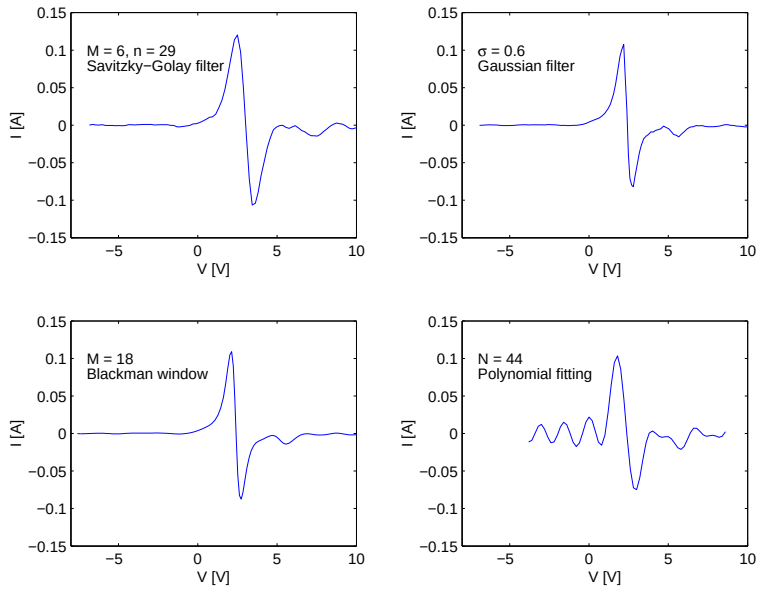

Figure 20: The second derivative of the LITH data set after smoothing by each of the methods.

Figure 20 shows the second derivative of the smaller data set measured at LITH and figure 21 the EEPF. The Gauss and Blackman methods produce a sharper maximum in the second derivative than the Savitzky-Golay. Again, polynomial fitting is not satisfactory. As before, there is distortion in the EEPF plots where the second derivative is close to zero. Testing with smaller Blackman window sizes and lower values of σ shows higher peaks in the second derivative. This indicates that for the values shown in fig-

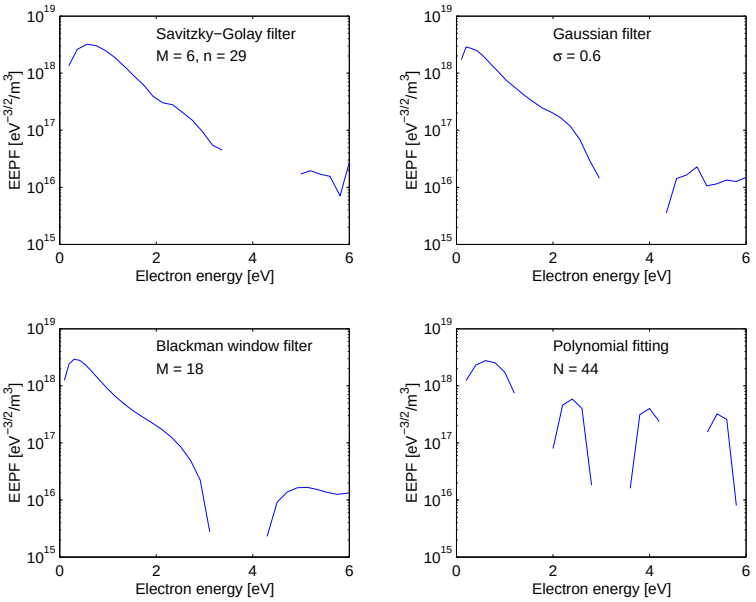

Figure 21: The electron energy probability function of the smoothed LITH data.

Method	T_{eff} [eV]	$T_{\text{eff}}^{\text{fit}}$ [eV]
Savitzky-Golay	0.8148	0.7489
Gaussian function	0.6054	0.5396
Blackman window	0.5733	0.5222
Polynomial fitting	NaN	NaN

Table 12: The effective electron temperature for the LITH data

ures 20 and 21 the filtering is causing some distortion which results in lower EEPF values. However, more filtering (larger window sizes and σ values) will preserve the shape of the EEPF for higher energies.

Table 12 shows the effective electron temperatures for the LITH data. As before the values for the Gaussian and Blackman filters are similar and $T_{\text{eff}}^{\text{fit}}$ is 9-10 % higher than T_{eff}. The values for the Savitzky-Golay are much higher and polynomial fitting did not produce results.

6 Conclusion

We have compared four methods for smoothing of a Langmuir probe I-V characteristic; the Savitzky-Golay filter, the Gaussian function filter, the Blackman window filter and polynomial fitting. Results show that the choice of method depends on the size of the data set as well as the noise level and

type.

The Savitzky-Golay filter performs extremely well when the noise level is moderate and the data is long enough to allow considerable cropping. In addition, the method produces the second derivative directly avoiding further error involved in numerical differentiation. Unequally spaced data can however pose problems and special measures must be taken [7] in order to avoid error. In addition, there are two parameters which must be decided upon, the polynomial degree and window size, and their choice is not transparent.

The Gaussian function filter gives consistent good results for both types of data tested here. There is however noticeable flattening of the maximum and minimum of the second derivative. The Gaussian filter is also particularly complicated to implement and considerable time went into finding a logical way to cut the output vectors to an equal length, keeping the voltage and current values correctly paired.

The Blackman window filter gives good results for both lengths of data. It achieves good smoothing at the cost of some flattening of the second derivative maximum and minimum. The Blackman window is a standard moving average window and is therefore extremely easy to adapt to any size of data and noise level. It is also resilient to other types of errors in the data such as digitising errors.

Polynomial fitting is an easy method to implement in a variety of computer programs. Testing indicated that the method might be a good choice for moderately noisy data but in reality it did not produce good results. In order to reproduce the sharp maximum and minimum it is necessary to use such a high degree that the polynomial also follows the noise to some extent.

All methods, except polynomial fitting, produce satisfactory results. The Blackman window filter combines ease of use with good smoothing for noisy data whereas the Savitzky-Golay combines minimal distortion of high frequency content and good smoothing for moderately noisy data.

Acknowledgments

The authors would like to thank professor Robert Magnus for help on various mathematical issues and professor Sven Sigurdsson for advice on Savitzky-Golay filtering. This work was partially supported by the University of Iceland Research Fund.

References

[1] V. A. Godyak, R. B. Piejak, and B. M. Alexandrovich, "Probe diagnostics of non-maxwellian plasmas," *Journal of Applied Physics*, vol. 73, pp. 3657 – 3663, 1993.

[2] V. A. Godyak, R. B. Piejak, and B. M. Alexandrovich, "Measurements of electron energy distribution in low-pressure rf discharges," *Plasma Sources Science and Technology*, vol. 1, pp. 36 – 58, 1992.

[3] M. J. Druyvesteyn, "Der niedervoltbogen," *Zeitschrift für Physik*, vol. 64, pp. 781 – 798, 1930.

[4] L.-F. Chi, K.-X. Lin, R.-H. Yao, X.-Y. Lin, C.-Y. Yu, and Y.-F. Yu, "Diagnostic of rf plasma by using Langmuir probe and its numerical processing," *Acta Physica Sinica*, vol. 50, pp. 1313 – 1317, 2001.

[5] K. F. Schoenberg, "Electron distribution function measurement by harmonically driven electrostatic probe," vol. 51, pp. 1159 – 1162, 1980.

[6] F. Fujita and H. Yamazaki, "Determination of electron energy distribution function of plasma by digital processing from Langmuir probe characteristic," *Journal of Applied Physics*, vol. 29, pp. 2139 – 2144, 1990.

[7] I. D. Sudit and R. C. Woods, "A workstation based Langmuir probe system for low-pressure dc plasmas," *Review of Scientific Instruments*, vol. 64, pp. 2440 – 2448, 1993.

[8] C. Lai, R. A. Breun, P. W. Sandstrom, A. E. Wendt, N. Hershkowitz, and R. C. Woods, "Langmuir probe measurements of electron temperature and density scaling in multidipole radio frequency plasmas," *Journal of Vacuum Science and Technology A*, vol. 11, pp. 1199–1205, 1993.

[9] T. Kimura, A. Yoneya, and K. Ohe, "Detection of electron energy distribution function by finite impulse response filter," *Japanese Journal of Applied Physics*, vol. 30, pp. 1877 – 1881, 1991.

[10] J. I. F. Palop, J. Ballesteros, V. Colomer, and M. A. Hernández, "A new smoothing method for obtaining the electron energy distribution function in plasma by the numerical differentiation of the *I-V* probe characteristic," *Review of Scientific Instruments*, vol. 66, pp. 4625 – 4636, 1995.

[11] J. T. Gudmundsson, "On smoothing of the *I-V* Langmuir probe characteristic." Memorandum No. UCB/ERL M97/38, Electron Research Laboratory, University of California, Berkeley, 1997.

[12] V. A. Godyak, "Measuring EEDF in gas discharge plasmas," in *Plasma-Surface Interactions and Processing of Materials* (O. Auciello, ed.), pp. 95 – 134, Dordrecht: Kluwer Academic Publishers, 1990.

[13] J. T. Gudmundsson, A. M. Marakhtanov, K. K. Patel, V. P. Gopinath, and M. A. Lieberman, "On the plasma parameters of a planar inductive oxygen discharge," *Journal of Physics D: Applied Physics*, vol. 33, pp. 1323–1331, 2000.

[14] J. T. Gudmundsson, J. Alami, and U. Helmersson, "Evolution of the electron energy distribution and the plasma parameters in a pulsed magnetron discharge," *Applied Physics Letters*, vol. 78, pp. 3427 – 3429, 2001.

[15] J. T. Gudmundsson, J. Alami, and U. Helmersson, "Spatial and temporal behavior of the plasma parameters in a pulsed magnetron discharge," *Surface and Coating Technology*, vol. 161, pp. 248–255, 2002.

[16] J. G. Laframboise and J. Rubinstein, "Theory of a cylindrical in a collisionless magnetoplasma," *Physics of Fluids*, vol. 19, pp. 1900 – 1908, 1976.

[17] E. Passoth, P. Kudrna, C. Csambal, J. F. Behnke, M. Tichý, and V. Helbig, "An experimental study of plasma density determination by a cylindrical Langmuir probe at different pressures and magnetic fields in a cylindrical magnetron discharge in heavy rare gases," *Journal of Physics D: Applied Physics*, vol. 30, pp. 1763–1777, 1997.

[18] M. A. Lieberman and A. J. Lichtenberg, *Principles of Plasma Discharges and Materials Processing*. New York: John Wiley & Sons, 1994.

[19] A. Savitzky and M. J. E. Golay, "Smoothing and differentiation of data by simplified least squares procedures," *Analytical Chemistry*, vol. 44, pp. 1627 – 1639, 1964.

[20] W. Gander and U. von Matt, "Smoothing filters," in *Solving Problems in Scientific Computing Using Maple and MATLAB* (W. Gander and J. Hřebíček, eds.), pp. 135 – 152, Berlin: Springer Verlag, 1997.

[21] W. H. Press and S. A. Teukolsky, "Savitzky-Golay smoothing filters," *Computers in Physics*, pp. 689 – 672, 1990.

[22] H. C. Hayden, "Data smoothing routine," *Computers in Physics*, vol. 1, pp. 74 – 75, 1987.

[23] L. B. Jackson, *Digital Filters and Signal Processing*. New York: Kluwer Academic Publishers, 1986.